

# Experimental and Theoretical Determination of the pH inside the Confinement of a Virus-Like Particle

Stan J. Maassen, Paul van der Schoot, and Jeroen J. L. M. Cornelissen\*

In biology, a variety of highly ordered nanometer-size protein cages is found. Such structures find increasing application in, for example, vaccination, drug delivery, and catalysis. Understanding the physiochemical properties, particularly inside the confinement of a protein cage, helps to predict the behavior and properties of new materials based on such particles. Here, the relation between the bulk solution pH and the local pH inside a model protein cage, based on virus-like particles (VLPs) built from the coat proteins of the cowpea chlorotic mottle virus, is investigated. The pH is a crucial parameter in a variety of processes and is potentially significantly influenced by the high concentration of charges residing on the interior of the VLPs. The data show a systematic more acidic pH of 0.5 unit inside the VLP compared to that of the bulk solution for pH values above pH 6, which is explained using a theoretical model based on a Donnan equilibrium. The model agrees with the experimental data over almost two orders of magnitude, while below pH 6 the experimental data point to a buffering capacity of the VLP. These results are a first step in a better understanding of the physiochemical conditions inside a protein cage.

## 1. Introduction

Over the years a variety of protein cages, in particular viruses, have been studied for their application in nanotechnology, which has yielded knowledge about their biological, chemical, and physical properties.<sup>[1–7]</sup> Due to their diversity, homogeneity, and well-defined dimensional properties, there is increasing interest in the use of viruses or virus-like particles (VLPs), for example, in the fields of biomedicine, materials science, and nanotechnology.<sup>[8–10]</sup> Some examples of this work involve

encapsulating non-native cargo such as enzymes,<sup>[11,12]</sup> polymers,<sup>[11,13,14]</sup> or metal nanoparticles.<sup>[15,16]</sup> Virus particles are also used for the formation of larger-scale structures.<sup>[17–19]</sup> Improving our understanding of viruses and VLPs is crucial to further advance this field and to find new applications for these particles.

A significant amount of data on the structure of many viruses is already available with sub-nanometer resolution. These data are commonly obtained by crystallography,<sup>[20–23]</sup> (cryo) electron microscopy,<sup>[24–27]</sup> and atomic force microscopy.<sup>[28–30]</sup> Furthermore, the physical properties of viruses, such as subunit interactions, assembly and disassembly behavior, and their response to environmental conditions have been extensively studied, both theoretically and experimentally.<sup>[2–4,31–34]</sup>

Still, many aspects concerning their physiochemical properties remain poorly understood. Even for the simplest viruses,

that is, those consisting of a single type of protein forming a capsid around the viral genetic material, the exact pathway for subunit assembly that leads to the formation of a virus particle is still under debate.<sup>[35]</sup> Furthermore, the effects of the protein cage on its cargo, for example, due to crowding of the cargo, the presence of high concentrations of charged species, or possible diffusion limitations across the capsid shell, are not fully understood.


We aim to gain insight in the physiochemical conditions inside a protein cage. Confinement effects may cause large differences in the physical conditions inside a capsid compared to those in bulk. For example, much work is done toward optimizing catalytic reactions inside protein cage structures.<sup>[36–40]</sup> Such processes are often strongly affected by the conditions, such as temperature, pH, and viscosity—under which they take place.

In order to obtain more insight in the interior physiochemical conditions of VLPs, we determine the pH on the inside of a VLP and relate this to the pH of the bulk solution. Many viruses rely on electrostatic interactions between a positively charged section of the coat protein and the negatively charged viral genetic material for capsid assembly and stability.<sup>[41,42]</sup> This means that after assembly a large number of charged species are concentrated on the inside of the capsid, which might influence the local proton concentration, that is, the pH. Previous studies already showed that the isoelectric point inside the PP7 virus capsid (pH  $\approx$  11.7) differs significantly from the isoelectric

S. J. Maassen, Prof. J. J. L. M. Cornelissen  
Laboratory of Biomolecular Nanotechnology  
MESA+ Institute for Nanotechnology  
University of Twente  
Enschede 7500 AE, The Netherlands  
E-mail: J.J.L.M.Cornelissen@utwente.nl

Prof. P. van der Schoot  
Group Theory of Polymers and Soft Matter  
Eindhoven University of Technology  
PO Box 513, 5600 MB Eindhoven, The Netherlands

Prof. P. van der Schoot  
Institute for Theoretical Physics  
Utrecht University  
Princetonplein 5, 3584 CC Utrecht, The Netherlands

 The ORCID identification number(s) for the author(s) of this article can be found under <https://doi.org/10.1002/sml.201802081>.

DOI: 10.1002/sml.201802081

point on the outside of the capsid ( $\text{pH} \approx 3.8$ ), yielding a difference in charge density between the inside and the outside.<sup>[43]</sup>

To investigate the pH conditions inside a virus capsid, we encapsulated a negatively charged pH-responsive polymer probe in a capsid formed by cowpea chlorotic mottle virus (CCMV) coat proteins (CPs). The pH probe is synthesized by including fluorescein methacrylate (FMA) subunits in a polystyrene sulfonate (PSS) polymer chain, forming fluorescein-containing PSS (FMA-PSS). Fluorescein and its derivatives are commonly used for pH-sensing purposes in biological systems due to their strong response in the near-neutral pH range.<sup>[44–46]</sup> The absorption spectrum and fluorescence emission of the fluorescein subunits are strongly pH-responsive, due to the different protonation states that the molecule can adopt.<sup>[47,48]</sup> At high pH, the fluorescence properties are mainly determined by the dianionic state, while upon lowering the pH the monoanionic state becomes more pronounced.<sup>[48]</sup> This allows for a ratiometric pH determination, using the ratio of the fluorescence emission intensity at an excitation wavelength corresponding to the monoanionic maximum excitation wavelength ( $\lambda \approx 490$  nm) divided by the emission intensity while exciting at the dianionic excitation wavelength ( $\lambda \approx 450$  nm). The probe that we use here has absorption maxima at  $\lambda = 458$  nm and  $\lambda = 499$  nm with an emission maximum of  $\lambda = 523$  nm. We use the ratio of fluorescence emission at  $\lambda_{\text{ex}} = 458$  nm compared to the fluorescence emission at  $\lambda_{\text{ex}} = 499$  nm as a measurement for the pH. Comparing the fluorescence response of the encapsulated probe with the response of the unencapsulated probe at various pHs gives an indication of the pH conditions inside the capsid. In order to explain the observed differences in pH inside the CCMV-based protein cage, we assumed a Donnan equilibrium of the charged species, which resulted in a model that correlates well in the relevant pH range.

## 2. Results and Discussion

### 2.1. FMA-PSS pH Sensitivity

To verify the sensitivity of FMA-PSS to pH changes, fluorescence spectra of the polymer solutions at a concentration of  $0.5 \text{ mg mL}^{-1}$  ( $\approx 25 \times 10^{-6} \text{ M}$ ) with pH varying from 5.0 to 7.5 (Figure 1) were obtained.

### 2.2. FMA-PSS Encapsulation

To test the pH response of FMA-PSS inside a VLP, the polymer was encapsulated inside CCMV-based VLPs by mixing the polymer with free CP dimers in solution at neutral pH (Figure 2).<sup>[39]</sup>

The formation of capsids was evident from size exclusion chromatography (SEC) with a UV-vis detector, which was also used for the purification of the VLPs (Figure 2a). The absorbance data are normalized to show an

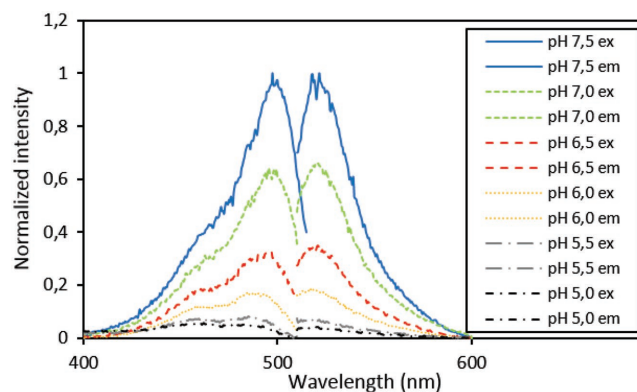


**Figure 1.** Excitation spectra at  $\lambda_{\text{em}} = 523$  nm showing excitation maxima at  $\lambda = 458$  nm and  $\lambda = 499$  nm at different pH. The ratio of the emission at  $\lambda = 523$  nm at  $\lambda_{\text{ex}} = 458$  nm and  $\lambda_{\text{ex}} = 499$  nm is used as a measure for the pH. Emission spectra at  $\lambda_{\text{ex}} = 499$  nm of FMA-PSS at various pH conditions. All spectra are normalized to the maximum intensity at pH 7.5 and point to an increased intensity at higher pH.

overlapping signal at the different detection wavelengths at an elution volume of  $V \approx 11$  mL, which is the characteristic elution volume for VLPs. The peak was isolated and analyzed by dynamic light scattering (DLS) and transmission electron microscopy (TEM) (Figure 2b,c). DLS showed that the isolated peak contains particles of  $19.0 \pm 3.8$  nm, which is confirmed by TEM analysis showing spherical particles with an average diameter of  $19.9 \pm 1.1$  nm. These data are in line with the previously confirmed  $T = 1$  icosahedral symmetry for CCMV VLPs formed at neutral pH on a polyanionic template.<sup>[38,49]</sup>

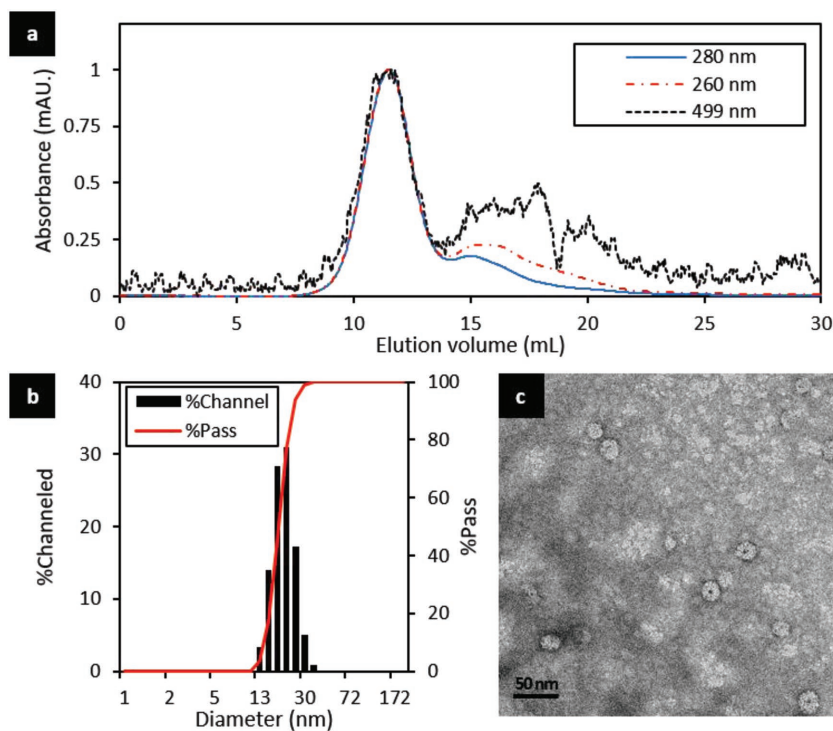


**Figure 2.** a) Normalized size exclusion chromatography (SEC) traces by UV-vis detection of the product formed after mixing FMA-PSS with CCMV CP at neutral pH. b) DLS and c) TEM analysis of the isolated particles after SEC.

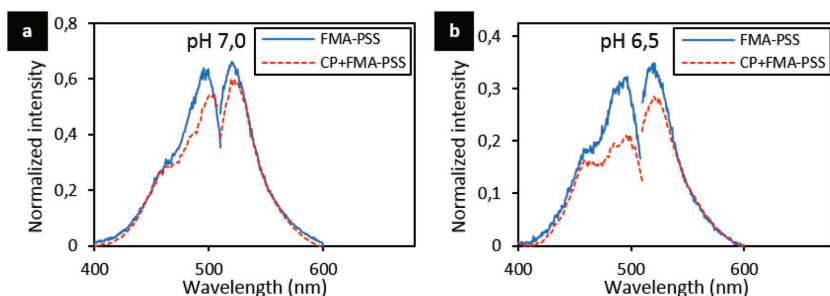


**Figure 3.** Comparison of the excitation spectra at  $\lambda_{em} = 523$  nm and emission spectra at  $\lambda_{ex} = 499$  nm of FMA-PSS in solution (blue, solid line) and encapsulated (red, broken line) FMA-PSS at a) pH 7.0 and b) pH 6.5.

The pH response of the FMA-PSS containing particles was measured using fluorescence spectroscopy over a range of pH values in which the VLPs are stable (pH 4–8), as was confirmed by DLS (see Figure S1, Supporting Information). Comparable to the polymer free in solution, the encapsulated polymer responded strongly to the changes in pH, becoming more fluorescent at higher pH (Figure S2, Supporting Information). Overlaying the excitation and emission spectra of FMA-PSS in solution and the encapsulated FMA-PSS at the same bulk solution pH clearly shows that the polymer responds differently in the two situations (Figure 3).

To further study the pH response of FMA-PSS in bulk solution and inside the VLPs, the ratio between the maximum emission at  $\lambda_{ex} = 458$  nm and the maximum emission at  $\lambda_{ex} = 499$  nm is compared. Since the protonation state of fluorescein is strongly dependent on the pH of the solution, the ratio of the emission at both excitation wavelengths is used as a measure for the pH of the solution.<sup>[47,48]</sup> In Figure 4, this ratio is plotted against the pH of the solution for both samples.

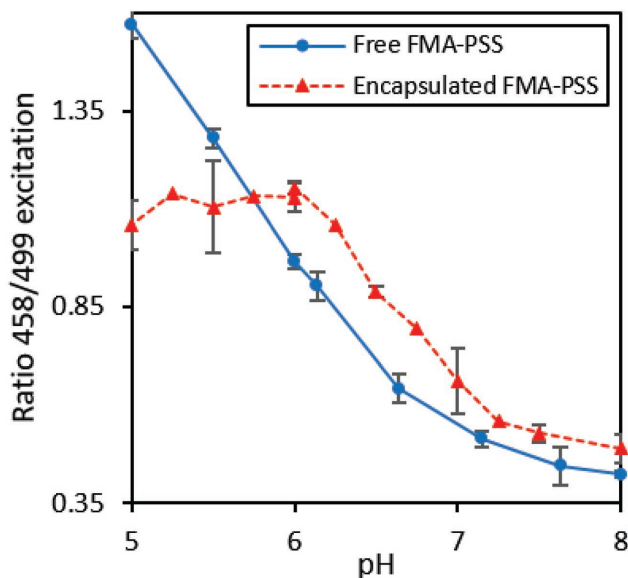


**Figure 4.** Ratio of maximum emission at  $\lambda_{ex} = 458$  nm and  $\lambda_{ex} = 499$  nm at varying pH for FMA-PSS free in solution (blue, solid line) and encapsulated FMA-PSS (red, broken line). All measurements were carried out in triplo.

The pH response of FMA-PSS inside a VLP is different from the pH response of FMA-PSS free in solution, as shown in Figure 4. Between pH 6.0 and 8.0 a pronounced shift is observed, corresponding to a more acidic environment for encapsulated FMA-PSS compared to free FMA-PSS. For example, the response of the polymer inside the capsid in a pH 6.5 buffer is similar to the free polymer in a pH 6.0 buffer. This suggests that within this range the polymer senses a more acidic environment inside the capsid than outside.

Between pH 5 and 6, the pH response inside the capsid is almost stable, whereas the free polymer still has a linear response in this range. The lack of change in response suggests that the degree of protonation of the fluorescein inside the capsid does not change in this range, implying a much smaller pH variation is sensed by the polymer inside the capsid than outside. This might be due to a buffering effect caused by the carboxylic acid pairs that increase the CP–CP interaction and stabilize the capsid.<sup>[50–52]</sup>

To investigate whether the observed response is caused by the encapsulation of the polymer rather than the presence of charged species, several control experiments were performed (Figure 5).

First of all, the response of the FMA-PSS in combination with CCMV CP lacking 26 amino acids on its N-terminus (CP $\Delta$ N26) was measured. The N-terminus can be cleaved from the unassembled CP upon prolonged standing. The absence of the N-terminus was confirmed by sodium dodecyl

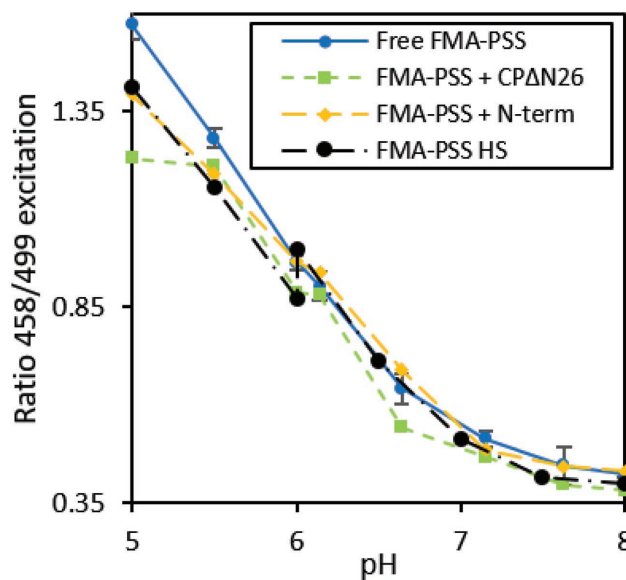


**Figure 5.** Ratio of maximum emission at  $\lambda_{ex} = 458$  nm and  $\lambda_{ex} = 499$  nm at varying pH for FMA-PSS free in solution (blue, solid line), FMA-PSS with CP $\Delta$ N26 in solution (green, short-dashed line), FMA-PSS with the N-terminal peptide fragment (N-term) in solution (orange, long-dashed line), and FMA-PSS with a high concentration of salt (1.8 M NaCl) in the solution (black, dashed-dotted line). All measurements were carried out in triplo.

sulfate (SDS), showing a reduction of protein mass by  $\approx 2$  kDa, matching the weight of the 26 amino acids (Figure S3, Supporting Information). These 26 amino acids, known as the arginine-rich motif (ARM), form the positively charged tail that points toward the inside of the CCMV capsid.<sup>[42]</sup> The ARM causes the interaction with negatively charged cargo; without that section, the protein–cargo interaction is reduced and cargo-templated assembly is no longer possible. However, assembly of CP $\Delta$ N26 can still occur at acidic pH. As can be seen from Figure 5, in the presence of CP $\Delta$ N26 the FMA-PSS responds similarly to the polymer free in solution between pH 5.5 and 8. Below pH 5.5, a deviation from the response of the free probe is observed. Comparable to the encapsulated probe, the probe mixed with CP $\Delta$ N26 shows a stable response at low pH, presumably caused by a buffering effect of the protein. Competition between the protonation of the protein and the protonation of the fluorescein causes a decreased pH response below pH 5.5 in comparison to the free polymer.

To specifically test the effect of the presence of the ARM, the pH response of FMA-PSS in the presence of a 26 amino acid peptide matching the ARM of CCMV CP (N26) was tested. The concentration of N26 was chosen such that it matches the local concentration inside a CCMV capsid. Similarly, to the case of CP $\Delta$ N26, the response of the polymer in the presence of N26 varied little from the polymer free in solution from pH 5.5 to 8. Below pH 5.5, a slight variation is again observed; however, it is less pronounced compared to CP $\Delta$ N26.

Finally, the effect of a high concentration of sodium chloride was studied, to test whether a high concentration of charged species affects the protonation of fluorescein at a pH < 5.5 (FMA-PSS HS). Under these conditions, the pH response of FMA-PSS was comparable to that of the polymer in the presence of N26. This suggests that the observed variations in the presence of N26 are indeed an effect of the high concentration of charged species.

In order to get an understanding of the molecular origin of the pH shift over the protein cage barrier, we developed a model to describe the acidity of the capsid cavity that is based on a Donnan equilibrium across the protein shell. To do this, we consider a virus capsid with a polyanionic cargo that interacts with the polycationic RNA-binding domains on the coat proteins lining the cavity of the protein shell. Complexation of the polycationic and polyanionic species does not necessarily lead to charge neutralization.<sup>[53–55]</sup> There are strong indications for overcharging, implying the total number of charges on the negatively charged species is larger than that on the positively charged species.<sup>[53,54]</sup> If indeed the case, this creates a Donnan potential across the protein shell that draws in mobile ionic species, in particular positively charged ones. This implies that the acidity inside the capsid must be lower than the acidity outside it.

This is confirmed by the next model: presume there are positively charged sodium ions, negatively charged chloride ions, and positively charged hydronium ions in the solution that acts as a reservoir for these species. Sodium and chloride ions are associated with added salt and in the model in addition act as counterions of the polyionic species present in the capsid's cavity as well as that for any acid present in the solution. Whether the actual ions present in the solution are sodium and chloride is irrelevant to the model, we merely take them for the sake of assigning names to them.

Let the mole fraction of these ions be denoted  $X_\alpha$  with  $\alpha = \text{Na}, \text{Cl}, \text{H}$ . The ions can freely move between the bulk solution and the cavity of the capsid through the holes in the shell that are known to be large enough to let ions pass.<sup>[52,56]</sup> Chemical equilibrium between the mobile ionic species across the shell presumes equal chemical potentials. This implies  $\ln X_\alpha^C \pm \phi = \ln X_\alpha^S$ , where the superscripts  $C$  and  $S$  indicate whether they refer to the capsid and solution regions, respectively. Here,  $\phi$  denotes the (dimensionless) Donnan potential, entering the equations with a positive sign for the positively charged species and with a negative sign for the negatively charged species. Note that any differences in reference chemical potential are tacitly absorbed in the Donnan potential.

This set of equations needs to be closed by insisting on charge neutrality inside the capsid and charge neutrality in the bulk solution. This gives additional equations  $X_{\text{Na}}^C - X_{\text{Cl}}^C + X_{\text{H}}^C - Q = 0$  and  $X_{\text{Na}}^S - X_{\text{Cl}}^S + X_{\text{H}}^S = 0$ . Here,  $Q$  is the net mole fraction of negative charges on the polyionic cargo. If  $Q < 0$ , then the cavity is undercharged, if  $Q > 0$ , it is overcharged. The mole fractions of the chlorine species and that of the hydronium species in the bulk solution are known quantities. The quantity  $Q$  we fix by fitting the measured acidities in the capsids and the bulk solution,  $\text{pH}^C$  and  $\text{pH}^S$ , to the theory. Charge neutrality sets  $X_{\text{Na}}^C$  and  $X_{\text{Na}}^S$ .

All other quantities can be expressed in terms of  $X_{\text{H}}^S$  and  $X_{\text{Cl}}^C$ . By solving the coupled set of equations, we find that the ratios  $X_{\text{Cl}}^C/X_{\text{Cl}}^S$  and  $X_{\text{H}}^C/X_{\text{H}}^S$  are inversely proportional, so  $X_{\text{H}}^C/X_{\text{H}}^S = X_{\text{Cl}}^C/X_{\text{Cl}}^S \equiv \alpha$ . Notice that  $\log \alpha = \text{pH}^S - \text{pH}^C$ . Furthermore, we find that  $\alpha = \exp \phi$  and that  $\alpha$  obeys a simple quadratic equation:  $\alpha^2 = 1 + (Q/X_{\text{Cl}}^S)\alpha$ . This already tells us that if the concentration of salt is sufficiently high and  $Q/X_{\text{Cl}}^S \ll 1$ , we have  $\alpha = 1$  and  $\text{pH}^S = \text{pH}^C$ . The quadratic equation can be solved exactly, to give  $\alpha = \frac{1}{2} (Q/X_{\text{Cl}}^S) + \frac{1}{2} \sqrt{(Q/X_{\text{Cl}}^S)^2 + 4}$ . Notice that this does not depend on the pH of the solution. This means the same shift of the pH in the capsid compared to that in the solution for all pH values.

The experimental shift of the pH found in experiments on CCMV coat proteins, encapsulating FMA-PSS in  $150 \times 10^{-3}$  M salt in  $T = 1$  particles, equals 0.37. This corresponds to  $\alpha = 2.3$ , and implies that  $(Q/X_{\text{Cl}}^S) = 1.9$ . To verify if this makes sense, we make use of the fact that a  $T = 1$  virus consists of 60 proteins, where the RNA-binding domains of each protein bear ten positive charges. In that case, we can write  $Q/X_{\text{Cl}}^S = \gamma \times (60 \times 10) / (N_A \times V_C \times [\text{NaCl}] \times 10^3)$ , where  $V_C = 4\pi R^3/3$  the volume of the cavity in  $\text{m}^3$ , with  $R$  its radius in m,  $N_A = 6 \times 10^{23} \text{ mol}^{-1}$  Avogadro's number, and  $[\text{NaCl}]$  the ionic strength in M. Here,  $\gamma$  is a number measuring the degree of overcharging. Estimating  $R = 4 \times 10^{-9}$  m, we get  $\gamma = 1.9/25 = 0.076$  implying an overcharging of a mere 8%. **Figure 6** shows the validity of the model between pH 6 and 8. At pH < 6 effects of the protein buffering come into play, which has not been accounted for in the model.

**Figure 6** shows that at pH > 6 the shift caused by the encapsulation is independent of the pH of the bulk solution. When shifting the response of the encapsulated probe (**Figure 6a**, red, dashed line) over the average pH difference between the free and the encapsulated probe between pH 6 and 7, it becomes



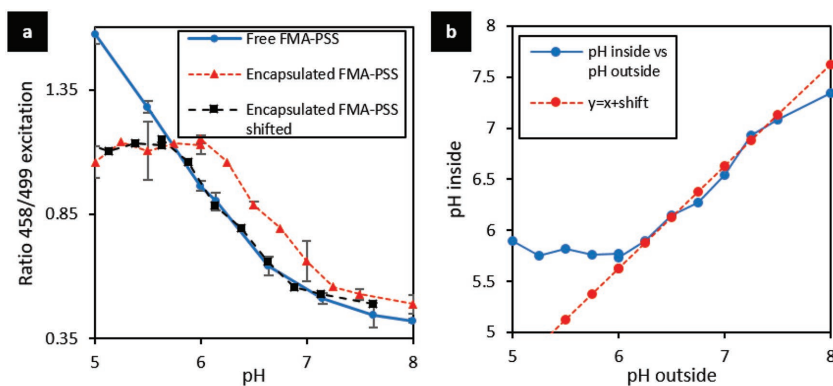


**Figure 6.** a) Ratio of maximum emission at  $\lambda_{\text{ex}} = 458$  nm and  $\lambda_{\text{ex}} = 499$  nm excitation at varying pH for FMA-PSS free in solution (blue, solid line), encapsulated FMA-PSS (red, broken line), and encapsulated FMA-PSS shifted over the average difference between pH 6 and 7 (black, broken line). All measurements were carried out in triplo. b) pH measured inside the capsid plotted against the bulk pH (blue, solid line), and the line pH inside = pH outside + the average shift between pH 6 and 7 (red, broken line).

clear that the trend in the response is similar to the free probe at pH above 6; the shifted encapsulated probe's response (Figure 6a, black, dashed line) and the free probe's response (Figure 6a, blue, solid line) overlap in this range. Figure 6b shows the line of the pH measured inside the capsids plotted against the bulk pH (Figure 6b, blue, solid line). Above pH 6 this line shows a linear trend that matches the line pH inside = pH outside + the average shift between pH 6 and 8, which further emphasizes that above pH 6 the encapsulation causes a pH shift that is independent of the bulk pH. This is in line with the outcome of the described model based on a Donnan equilibrium.

### 3. Conclusion

In order to better understand the physicochemical conditions inside a model protein cage, we measured the pH inside a virus-like particle and compared it to the bulk solution conditions. The obtained data show that the pH inside such a capsid is  $\approx 0.5$  more acidic between pH 6 and 8, while at pH < 6 the measured response inside the capsid remains constant. The observed shift can be explained by a simple model based on a Donnan equilibrium over the protein shell. This model suggests a slight negative overcharging of the capsid of  $\approx 8\%$ , and explains the experimental pH shift inside the capsid compared to the bulk pH.

Insight in the physicochemical conditions inside nanometer-size protein cages is crucial for a better understanding of the assembly and disassembly processes of these containers, but also their biological relevance. Furthermore, it will be of aid in the design and synthesis of artificial, for example, virus-based, protein cages that find application in nanoreactors, materials, and medicine. The presented combination of experimental and theoretical analyses yield insight that can potentially be generalized to other protein cages, beyond the CCMV VLP discussed in this contribution. While the encased polymer probe gave us insight in the increased acidity inside the CCMV VLP as a function of the bulk pH, only with the help of the theoretical model

we were able to present a chemical mechanistic explanation in terms of a Donnan potential caused by the charge imbalance between the cationic RNA-binding domains of the CCMV CPs and the encapsulated polyanions.

### 4. Experimental Section

**Materials:** All chemicals were purchased from Sigma Aldrich and used without further purification. The wild-type CCMV virus was obtained according to literature procedures.<sup>[57,58]</sup> Solutions were prepared using Milli-Q water (Millipore, 18.2 m $\Omega$ ).

**Synthesis of the FMA-PSS pH Probe:** 878.4 mg of NaSS (4.26 mmol), 85 mg of FMA (0.21 mmol), and 14  $\mu$ L of (BIBOEt)<sub>2</sub>S<sub>2</sub> (20.7 mg, 0.0457 mmol) were dissolved in 4.2 mL of Milli-Q water. This solution was purged with N<sub>2</sub> gas for 45 min. An excess amount of MeOH was also purged with N<sub>2</sub> gas for 45 min. Next, 1.4 mL of purged MeOH was added to the aqueous solution using a N<sub>2</sub>-purged syringe. The solution was purged with N<sub>2</sub> gas for an additional 5 min before adding 13.6 mg Cu(I)Br (0.095 mmol) and 29.6 mg BPY (0.19 mmol) as a solid while maintaining a N<sub>2</sub> gas purge. After addition of the catalyst, the reaction mixture turned brown, and was stirred under N<sub>2</sub> atmosphere for 48 h at room temperature (RT). After 48 h, the reaction was terminated by opening the flask, causing the reaction mixture to turn from brown to blue indicating oxidation of the Cu(I) catalyst to Cu(II). The copper was removed by running the mixture over a silica gel column (eluent 1:1 H<sub>2</sub>O:MeOH). After that, the polymer was precipitated from tetrahydrofuran (THF). The precipitated solid was filtered off, redissolved in 1:1 H<sub>2</sub>O:MeOH and again precipitated from THF. The purified polymer was dried for 12 h at 60 °C before analysis using NMR, high-performance liquid chromatography (HPLC) (see Figure S4, Supporting Information), UV-vis spectroscopy, and fluorescence spectroscopy.

**Cowpea Chlorotic Mottle Virus Coat Protein Isolation:** The CP of CCMV was isolated according to procedures described in the literature.<sup>[57,58]</sup> Wild-type CCMV dissolved in virus buffer (100  $\times 10^{-3}$  M NaOAc; 1  $\times 10^{-3}$  M ethylenediaminetetraacetic acid (EDTA); 1  $\times 10^{-3}$  M NaN<sub>3</sub>; pH 5.0) with a concentration of  $\approx 10$  mg mL<sup>-1</sup> was dialyzed against protein isolation buffer (50  $\times 10^{-3}$  M Tris; 500  $\times 10^{-3}$  M CaCl<sub>2</sub>; pH 7.5) using 12–14 kDa dialysis membranes for at least 8 h, during which the buffer was replaced twice. Next, the precipitated RNA was removed centrifugation at 40 000 rpm at 4 °C for 2 h using a Sorvall WX80 ultracentrifuge. The supernatant containing CP dimers were dialyzed for 3 h against cleaning buffer (50  $\times 10^{-3}$  M Tris; 500  $\times 10^{-3}$  M NaCl; pH 7.5), followed by dialysis to PSS encapsulation buffer (50  $\times 10^{-3}$  M Tris; 300  $\times 10^{-3}$  M NaCl; pH 7.5) for 5 h with 1 $\times$  buffer replacement. The CP was used within 2 d after isolation, and to ensure protein purity only CP solutions that had a 280/260 nm absorbance ratio of at least 1.5 were used.

**Removing N-Terminus from Coat Protein:** For experiments involving CP missing a part of its N-terminus (CPAN26), the N-terminus was removed as described before.<sup>[59]</sup> Here, CPAN26 was prepared by dialyzing isolated CP against PSS encapsulation buffer (50  $\times 10^{-3}$  M Tris; 300  $\times 10^{-3}$  M NaCl; pH 7.5) for at least two weeks. After that, the CP was purified using size-exclusion chromatography (SEC), and analyzed by sodium dodecyl sulfate polyacrylamide gel electrophoresis (SDS-PAGE).

**FMA-PSS Encapsulation in Cowpea Chlorotic Mottle Virus Virus-Like Particles:** CP (5–10 mg mL<sup>-1</sup>) in PSS encapsulation buffer (50  $\times 10^{-3}$  M Tris; 300  $\times 10^{-3}$  M NaCl; pH 7.5) was mixed 1:1 into a solution of FMA-PSS in Milli-Q water (weight ratio CP:FMA-PSS = 2.4:1). The mixture was

stirred at 4 °C for 1 h. The VLPs formed were purified using size-exclusion chromatography using a 2× diluted PSS encapsulation buffer (25 × 10<sup>-3</sup> M Tris; 150 × 10<sup>-3</sup> M NaCl; pH 7.5) as eluent. After SEC, the VLPs were concentrated using spin filtration and analyzed using DLS, TEM, UV-vis spectroscopy, and fluorescence spectroscopy.

**pH Measurements inside Virus-Like Particles:** For pH measurements inside VLPs, the purified FMA-PSS containing VLPs were dialyzed to a phosphate buffer (25 × 10<sup>-3</sup> M phos; 150 × 10<sup>-3</sup> M NaCl, pH 6.0–8.0) or acetate buffer (25 × 10<sup>-3</sup> M NaOAc; 150 × 10<sup>-3</sup> M; 4.0–6.0) of the desired pH, ranging from 4 to 8, using a volume ratio of sample to buffer of at least 1000. The VLPs were concentrated to a concentration of ≈1.5 mg mL<sup>-1</sup>, giving a sufficiently high concentration to be able to measure fluorescence at acidic pH. DLS and UV-vis spectroscopy measurements were performed to check the particle size and concentration. Fluorescence spectroscopy was used to obtain excitation and emission spectra over a range of pH. Excitation spectra were measured using an emission wavelength of λ<sub>em</sub> = 523 nm and emission spectra were measured using both λ<sub>ex</sub> = 458 and 499 nm excitation wavelengths.

Control experiments involving CP missing a part of its N-terminus (CPΔN26) were performed using a similar procedure except that CP was replaced by CPΔN26.

**pH Measurements in Buffer:** For pH measurements in buffer 1 mg mL<sup>-1</sup> FMA-PSS in Milli-Q water was mixed 1:1 with a phosphate buffer (50 × 10<sup>-3</sup> M phos; 300 × 10<sup>-3</sup> M NaCl; pH 6.0–8.0) or acetate buffer (50 × 10<sup>-3</sup> M NaOAc; 300 × 10<sup>-3</sup> M NaCl; pH 4.0–6.0) of the desired pH. UV-vis spectroscopy was performed to compare the FMA concentrations in the solutions and fluorescence spectroscopy was used to obtain excitation and emission spectra over a range of pH. Excitation spectra were measured using an emission wavelength of 523 nm and emission spectra were measured using both λ = 458 and 499 nm excitation wavelengths.

Control experiments involving only the last 26 amino acids of the N-terminus of the CP (N26) or involving high ionic strength were performed following the same procedure as used for the pH measurements in buffer, except for the addition of N26 (0.32 × 10<sup>-3</sup> M) or the addition of NaCl (final NaCl concentration in experiment = 1.8 M), respectively, to the solutions in these control experiments.

## Supporting Information

Supporting Information is available from the Wiley Online Library or from the author.

## Acknowledgements

The authors acknowledge financial support from the ERC Consolidator Grant (ProtCage) to J.J.L.M.C. The authors are grateful to Dr. E. G. Keim (MESA+ Institute for Nanotechnology, University of Twente) for assistance with TEM.

## Conflict of Interest

The authors declare no conflict of interest.

## Keywords

confinement, nanotechnology, pH measurements, physical chemistry, virus capsids

Received: May 31, 2018

Revised: July 17, 2018

Published online: August 13, 2018

- [1] A. M. L. Lever, K. T. Jeang, *Int. J. Hematol.* **2006**, *84*, 23.
- [2] T. Douglas, M. Young, *Nature* **1998**, *393*, 152.
- [3] D. L. Caspar, A. Klug, *Cold Spring Harbor Symp. Quant. Biol.* **1962**, *27*, 1.
- [4] L. Lavelle, M. Gingery, M. Phillips, W. M. Gelbart, C. M. Knobler, R. D. Cadena-Nava, J. R. Vega-Acosta, L. A. Pinedo-Torres, J. Ruiz-Garcia, *J. Phys. Chem. B* **2009**, *113*, 3813.
- [5] M. G. Mateu, *Virus Res.* **2012**, *168*, 1.
- [6] J. Snijder, O. Kononova, I. M. Barbu, C. Uetrecht, W. F. Rurup, R. J. Burnley, M. S. T. Koay, J. J. L. M. Cornelissen, W. H. Roos, V. Barsagom, G. J. L. Wuite, A. J. R. Heck, *Biomacromolecules* **2016**, *17*, 2522.
- [7] A. Tamura, Y. Fukutani, T. Takami, M. Fujii, Y. Nakaguchi, Y. Murakami, K. Noguchi, M. Yohda, M. Odaka, *Biotechnol. Bioeng.* **2015**, *112*, 13.
- [8] P. Singh, M. J. Gonzalez, M. Manchester, *Drug Dev. Res.* **2006**, *67*, 23.
- [9] A. G. Malyutin, R. Easterday, Y. Lozovyy, A. Spilotos, H. Cheng, O. R. Sanchez-Felix, B. D. Stein, D. G. Morgan, D. I. Svergun, B. Dragnea, L. M. Bronstein, *Chem. Mater.* **2015**, *27*, 327.
- [10] C. M. Soto, B. R. Ratna, *Curr. Opin. Biotechnol.* **2010**, *21*, 426.
- [11] F. D. Sikkema, M. Comellas-Aragonès, R. G. Fokkink, B. J. M. Verduin, J. J. L. M. Cornelissen, R. J. M. Nolte, *Org. Biomol. Chem.* **2007**, *5*, 54.
- [12] Z. Zhao, J. Fu, S. Dhakal, A. Johnson-Buck, M. Liu, T. Zhang, N. W. Woodbury, Y. Liu, N. G. Walter, H. Yan, *Nat. Commun.* **2016**, *7*, 10619.
- [13] M. Comellas-Aragonès, A. De La Escosura, A. J. Dirks, A. Van Der Ham, A. Fusté-Cuñé, J. J. L. M. Cornelissen, R. J. M. Nolte, *Biomacromolecules* **2009**, *10*, 3141.
- [14] S. J. Maassen, A. M. Van Der Ham, J. J. L. M. Cornelissen, *ACS Macro Lett.* **2016**, *5*, 987.
- [15] I. Tsvetkova, C. Chen, S. Rana, C. C. Kao, V. M. Rotello, B. Dragnea, *Soft Matter* **2012**, *8*, 4571.
- [16] L. Loo, R. H. Guenther, S. A. Lommel, S. Franzen, *J. Am. Chem. Soc.* **2007**, *129*, 11111.
- [17] M. A. Kostianen, P. Hiekkataipale, A. Laiho, V. Lemieux, J. Seitonen, J. Ruokolainen, P. Ceci, *Nat. Nanotechnol.* **2013**, *8*, 52.
- [18] K. T. Nam, D. W. Kim, P. J. Yoo, C. Y. Chiang, N. Meethong, P. T. Hammond, Y. M. Chiang, A. M. Belcher, *Science* **2006**, *312*, 885.
- [19] N. F. Steinmetz, K. C. Findlay, T. R. Noel, R. Parker, G. R. Lomonosoff, D. J. Evans, *ChemBioChem* **2008**, *9*, 1662.
- [20] K. Valegård, L. Liljas, K. Fridborg, T. Unge, *Nature* **1990**, *345*, 36.
- [21] M. G. Rossmann, *Q. Rev. Biophys.* **2013**, *46*, 133.
- [22] J. M. Hogle, M. Chow, D. J. Filman, *Science* **1985**, *229*, 1358.
- [23] D. Veessler, B. M. Kearney, J. E. Johnson, *Crystallogr. Rev.* **2016**, *22*, 102.
- [24] N. Grigorieff, S. C. Harrison, *Curr. Opin. Struct. Biol.* **2011**, *21*, 265.
- [25] C. Plisson, M. Uzest, M. Drucker, R. Froissart, C. Dumas, J. Conway, D. Thomas, S. Blanc, P. Bron, *J. Mol. Biol.* **2005**, *346*, 267.
- [26] J. A. Speir, S. Munshi, G. Wang, T. S. Baker, J. E. Johnson, *Structure* **1995**, *3*, 63.
- [27] R. I. Koning, J. Gomez-Blanco, I. Akopjana, J. Vargas, A. Kazaks, K. Tars, J. M. Carazo, A. J. Koster, *Nat. Commun.* **2016**, *7*, 12524.
- [28] H. Maeda, *Langmuir* **1997**, *13*, 4150.
- [29] D. Martinez-Martin, C. Carrasco, M. Hernando-Perez, P. J. de Pablo, J. Gomez-Herrero, R. Perez, M. G. Mateu, J. L. Carrascosa, D. Kiracofe, J. Melcher, A. Raman, *PLoS One* **2012**, *7*, e30204.
- [30] A. J. Malkin, A. McPherson, P. D. Gershon, *J. Virol.* **2003**, *77*, 6332.
- [31] J. B. Bancroft, E. Hiebert, M. W. Rees, R. Markham, *Virology* **1968**, *34*, 224.
- [32] J. D. Perlmutter, M. R. Perkett, M. F. Hagan, *J. Mol. Biol.* **2014**, *426*, 3148.
- [33] P. Van Der Schoot, R. Zandi, *Phys. Biol.* **2007**, *4*, 296.

- [34] D. Endres, A. Zlotnick, *Biophys. J.* **2002**, *83*, 1217.
- [35] R. F. Garmann, M. Comas-Garcia, C. M. Knobler, W. M. Gelbart, *Acc. Chem. Res.* **2016**, *49*, 48.
- [36] I. J. Minten, V. I. Claessen, K. Blank, A. E. Rowan, R. J. M. Nolte, J. J. L. M. Cornelissen, *Chem. Sci.* **2011**, *2*, 358.
- [37] D. P. Patterson, P. E. Prevelige, T. Douglas, *ACS Nano* **2012**, *6*, 5000.
- [38] L. Schoonen, J. C. M. Van Hest, *Adv. Mater.* **2016**, *28*, 1109.
- [39] M. Brasch, R. M. Putri, M. V. De Ruitter, D. Luque, M. S. T. Koay, J. R. Castón, J. J. L. M. Cornelissen, *J. Am. Chem. Soc.* **2017**, *139*, 1512.
- [40] J. D. Fiedler, S. D. Brown, J. L. Lau, M. G. Finn, *Angew. Chem., Int. Ed.* **2010**, *49*, 9648.
- [41] V. A. Belyi, M. Muthukumar, *Proc. Natl. Acad. Sci. USA* **2006**, *103*, 17174.
- [42] R. F. Garmann, M. Comas-Garcia, M. S. Koay, J. J. L. M. Cornelissen, C. M. Knobler, W. M. Gelbart, *J. Virol.* **2014**, *88*, 10472.
- [43] R. J. Nap, A. L. Božič, I. Szleifer, R. Podgornik, *Biophys. J.* **2014**, *107*, 1970.
- [44] R. Wang, C. Yu, F. Yu, L. Chen, C. Yu, *TrAC, Trends Anal. Chem.* **2010**, *29*, 1004.
- [45] C. Peng, W. Hu, Y. Zhou, C. Fan, Q. Huang, *Small* **2010**, *6*, 1686.
- [46] H. N. Kim, K. M. K. Swamy, J. Yoon, *Tetrahedron Lett.* **2011**, *52*, 2340.
- [47] J. Han, K. Burgess, *Chem. Rev.* **2010**, *110*, 2709.
- [48] R. Sjöback, J. Nygren, M. Kubista, *Spectrochim. Acta, Part A* **1995**, *51*, L7.
- [49] R. D. Cadena-Nava, Y. Hu, R. F. Garmann, B. Ng, A. N. Zelikin, C. M. Knobler, W. M. Gelbart, *J. Phys. Chem. B* **2011**, *115*, 2386.
- [50] D. L. D. Caspar, in *Advances in Protein Chemistry*, Vol. 18 (Eds: C. B. Anfinsen, M. L. Anson, J. T. Edsall), Academic, San Diego, CA **1964**, pp. 37–121.
- [51] H. Liu, C. Qu, J. E. Johnson, D. A. Case, *J. Struct. Biol.* **2003**, *142*, 356.
- [52] J. B. Bancroft, G. J. Hills, R. Markham, *Virology* **1967**, *31*, 354.
- [53] S. Li, G. Erdemci-Tandogan, J. Wagner, P. Van Der Schoot, R. Zandi, *Phys. Rev. E* **2017**, *96*, 022401.
- [54] J. D. Perlmutter, C. Qiao, M. F. Hagan, *eLife* **2013**, *2*, e00632.
- [55] S. W. Singaram, R. F. Garmann, C. M. Knobler, W. M. Gelbart, A. Ben-Shaul, *J. Phys. Chem. B* **2015**, *119*, 13991.
- [56] L. O. Liepold, J. Revis, M. Allen, L. Oltrogge, M. Young, T. Douglas, *Phys. Biol.* **2005**, *2*, S166.
- [57] M. Comellas-Aragones, H. Engelkamp, V. I. Claessen, N. A. J. M. Sommerdijk, A. E. Rowan, P. C. M. Christianen, J. C. Maan, B. J. M. Verduin, J. J. L. M. Cornelissen, R. J. M. Nolte, *Nat. Nanotechnol.* **2007**, *2*, 635.
- [58] B. J. M. Verduin, *FEBS Lett.* **1974**, *45*, 50.
- [59] J. Mikkilä, A.-P. Eskelinen, E. H. Niemelä, V. Linko, M. J. Frilander, P. Törmä, M. A. Kostainen, *Nano Lett.* **2014**, *14*, 2196.